Improved signature prediction through coupling of ShipIR and CFD

David A. Vaitekunas[a,1], Chris Sideroff[b,2], Christine Moussa[a]

[a]W.R. Davis Engineering Limited, 1260 Old Innes Road, Ottawa, Ontario, Canada K1B 3V3
[b]Pointwise, Inc., 213 S. Jennings Ave., Ft Worth, TX 76114 USA

ABSTRACT

Most existing platform signature models use semi-empirical correlations to predict flow convection on internal and external surfaces, a key element in the prediction of accurate skin signature. Although these convection algorithms are capable of predicting bulk heat transfer coefficients between each surface and the designated flow region, they are not capable of capturing local effects such as flow stagnation, flow separation, and flow history. Most computational fluid dynamics (CFD) codes lack the ability to predict changes in background solar and thermal irradiation with the environment and sun location, nor do they include multi-bounce radiative surface exchanges by default in their solvers. Existing interfaces between CFD and signature prediction typically involve a one-directional mapping of CFD predicted temperatures to the signature model. This paper describes a new functional interface between the NATO-standard ship signature model (ShipIR) and the ANSYS Fluent model, where a bi-directional mapping is used to transfer the thermal radiation predictions from ShipIR to Fluent, and after re-iteration of the CFD solution, transfer the wall and fluid temperatures back to ShipIR for further refinement of local-area heat transfer coefficients, and re-iteration of the ShipIR thermal solution. Both models converge to an RMS difference of 0.3 °C within a few successive iterations (5–6). This new functional interface is described through a detailed thermal/IR simulation of an unclassified research vessel, the Canadian Forces Auxiliary Vessel (CFAV) Quest. Future efforts to validate this new modelling approach using shipboard measurements are also discussed.

Keywords: thermal solver, infrared signature, CFD, convection, radiation, coupled solution, background irradiation

2. INTRODUCTION

ShipIR/NTCS is a comprehensive software engineering tool for predicting the thermal infrared (IR) signature and IR susceptibility of naval warships. The ShipIR component consists of several sub-models, including the MODTRAN4 infrared sky radiance and atmosphere propagation model, a proprietary sea reflectance model combining the methods of Mermelstein (1994) with the results from Shaw and Churnside (1997) and Ross and Dion (2007). The platform model is created from a 3D surface geometry that forms the basis of both a radiative heat transfer and in-band surface radiance model comprised of diffuse and specular multi-bounce reflections. An exhaust plume trajectory and IR emission model predicts the infrared signature of diesel engine and gas turbine exhaust systems. Internal heat sources are modelled via user-defined thermal boundary conditions, simulating a complex thermal network of specified temperatures (controlled spaces), forced and natural

---

[1] dvaitekunas@davis-eng.com; http://www.davis-eng.com; phone: +1 613 748 5500; fax: +1 613 748 3972

[2] cnsidero@pointwise.com; http://www.pointwise.com/free; phone: +1 800 4PTWISE
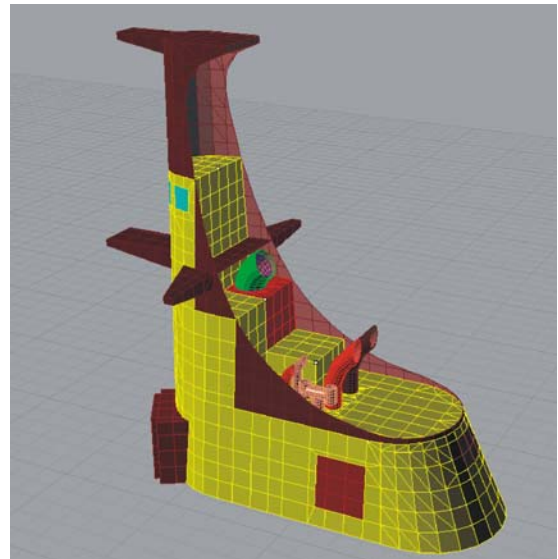
Figure 1: ShipIR model of CFAV Quest.

Figure 2: ShipIR mesh of funnel and mast.

convection, heat-flux, and heat conduction. Validation of the ShipIR model has been the topic of several research papers (Vaitekunas and Fraedrich 1999, Fraedrich et al. 2003, Vaitekunas 2005).

The ShipIR model of the Canadian Forces Auxiliary Vessel (CFAV) Quest, shown in Figure 1, was chosen as a test article for the development of this new interface between ShipIR and Fluent CFD. The fluid volume around the funnel and mast areas were modelled first, as illustrated in Figure 2, to test the functional interface before attempting to model the full-ship fluid volume.

Table 1: Propulsion, hotel power, and ventilation conditions.

ID	Description	Power (kW)	flow (kg/s)	Temp (°C)
mpde	10 cyl. Fairbanks-Morse 38D8	1110	3.61	323
gt	Solar Saturn gas turbine	750	5.53	443
ssdg	Caterpillar diesel generator	150	0.57	164
mmr-in	main machinery air intakes		6.34	26.4
gt-in	gas turbine air intake		5.45	26.4
mmr-out	machinery compartment air outlet		4.49	30

The funnel area was selected because it has a total of seven exhaust outlets: 2 main propulsion diesel engines (MPDE), 2 ship service diesel generators (SSDG), 1 gas turbine (GT), 1 ship emergency diesel generator (SEDG), and 1 T-shaped boiler exhaust chimney. It also has four air inlet vents (2 main machinery compartment air inlets, 1 GT air intake, 1 GT silencer air intake) and two air outlet vents (1 main machinery compartment air outlet, 1 silencer air outlet around the circumference of the GT exhaust outlet). The inlet flow conditions specified on each outlet and inlet are summarized in Table 1. The Quest is a diesel electric ship, and although the two MPDEs and GT are specified to be operating at full-power in this simulation, in reality only either the MPDE(s) or the GT can be connected to the two GE drive motors. This fictitious arrangement was configured to analyse all the exhaust plumes simultaneously. The inlet conditions to the boiler and SEDG uptake were left out of the simulation, but the air intakes and outlets are specified based on fan speed and air consumption by each engine. The ship and ambient inputs used are summarized in Table 2. The wind speed and direction relative to the ship are 3.22 m/s and 326.2° (CW from bow). The ship is located at (65°E, 20°N) on 15 April at 03h36 GMT, resulting in a sun azimuth of 90.8° (from TN) and elevation of 30°. These result in a sun azimuth, relative to the ship, of 310.8° (CW from bow).

The CFD surface and volume meshes were created from the exported ShipIR mesh shown in Figure 2, using Gridgen (Pointwise). These meshes were constructed by Pointwise Inc. and re-exported as a Fluent case file. The Gridgen surface

Table 2: Ship and ambient inputs.

Variable	Description	Value
V_s	Ship speed (kts)	14.5
ϕ_s	Ship heading (°CW from TN)	140
V_w	Wind speed (kts)	20
ϕ_w	Wind direction (°CW from TN)	310
T_{air}	Air temperature (°C)	26.4
T_{sea}	Sea temperature (°C)	27
RH	Relative humidty (%)	67

Figure 3: CFD surface mesh created using Pointwise.

Figure 4: Volume mesh along two principal planes (from Fluent).

mesh is shown in Figure 3 and the fluid volume mesh in the vicinity of the funnel is shown in Figure 4 using top (xy) and side (xz) planes through the volume at (0,0,13) m.
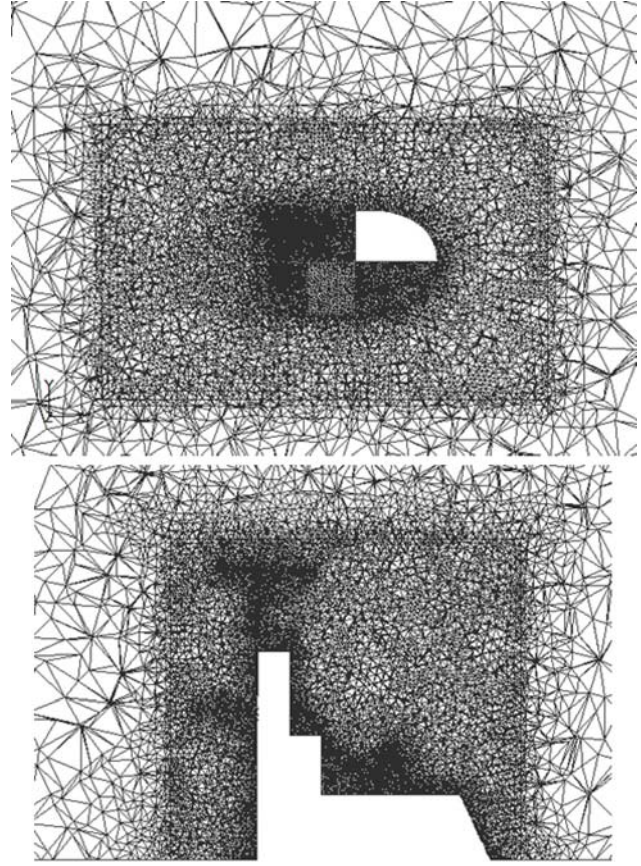
3. SHIPIR THERMAL MODEL

The ShipIR thermal model is based on a steady-state solution of the generalized Fourier heat conduction equation:

$$C\frac{\partial T}{\partial t} + K\frac{\partial^2 T}{\partial x_i^2} + S = 0 \quad \rightarrow \quad K\frac{\partial^2 T}{\partial x_i^2} + S = 0 \tag{1}$$

When applied to a control volume with a thin-wall assumption, the following finite difference equation is obtained:

$$\sum_{j}^{N_j} C_{ij}(T_i - T_j) + \sum_{k}^{N_k} Q_{ik} = 0 \tag{2}$$

The following two conductance terms are used to model conduction and convection:

$$C_{ij} = \begin{cases} (KA/t)_{ij} \\ (hA)_{ij} \end{cases} \tag{3}$$

The surface area (A_{ij}) is perpendicular to the direction of heat flow, the thickness (t_{ij}) is measured along the path between T_i and T_j, K is the thermal conductivity (W/m°C) of the material, and h is the convective heat transfer coefficient (W/m²°C) of the fluid. The heat source terms (S, Q_{ik}) are external heat fluxes imposed on the surface. They include radiation, condensation, evaporation and other user-defined boundary conditions (window heaters, thermal dissipation from combat and sensor systems, etc.). The net radiative flux on each kth surface of the ith thermal node is computed by ShipIR using the following surface radiosity (J_k) formulation:

$$J_{k\lambda} = \varepsilon_{k\lambda} E_{b\lambda}(T_i) + \rho_{k\lambda} G_{k\lambda} \tag{4}$$

which includes direct thermal emissions from the plate (E_b) and any reflected irradiation (G_k):

$$G_{k,\lambda} = F_{k,a} E_{bck,\lambda}(\theta_k) + \sum_{j}^{N_{kj}} F_{k,j} J_{j,\lambda} + F_{k,sun} E_{sun,\lambda}(\phi_s, \theta_s) + F_{k,a} E_{sol,\lambda}(\phi_k, \theta_k) \tag{5}$$

These include thermal irradiation from the background (E_{bck}), direct sun (E_{sun}) and indirect solar (E_{sol}) irradiation, and any net radiosity (J_j) from the surrounding surfaces (i.e., multi-bounce radiation). Indirect solar irradiation includes atmosphere and sea reflected sunlight. The radiation view factor ($F_{k,j}$) defines the fraction of radiative energy leaving surface (j) and irradiating surface (k):

$$F_{k,j} = \frac{1}{A_k} \int_{A_k} \int_{A_j} \frac{\cos\theta_k \cos\theta_j}{\pi r^2} dA_k dA_j \tag{6}$$

The radiation view factors are computed by ShipIR using RAVFAC. Two additional view factors are computed by ShipIR:

$$F_{k,a} = 1 - \sum_{j}^{N_j} F_{k,j} \tag{7}$$

$$F_{k,sun} = C_{k,sun} \bar{n}(\phi_k, \theta_k) \cdot \bar{n}(\phi_s, \theta_s) \tag{8}$$

$F_{k,a}$ is the remainder of the hemisphere not occupied by surfaces and assumed to be the background. $C_{k,sun}$ is the fraction of each surface exposed to the sun (to account for geometric shadowing). The net radiative heat flux is the difference between outgoing and incoming irradiation:

$$q_{k,\lambda} = J_{k,\lambda} + \tau_{k,\lambda} G_{k,\lambda} - G_{k,\lambda} \tag{9}$$

After substituting for radiosity and surface transmission (i.e., windows), the following radiative transfer equation is obtained:

$$q_{k,\lambda} = \varepsilon_{k,\lambda} \left[E_{b,\lambda}(T_i) - G_{k,\lambda} \right] \tag{10}$$

Since the radiative emissions from earth-bound temperature sources (T=thermal) and the sun (s=solar) are spectrally segregated (see Figure 5), the spectral integrity of the radiative energy is conserved by ShipIR using the following two-band formulation:

$$q_k = \alpha_{k,S} \left[0 - G_{k,sol} \right] + \varepsilon_{k,T} \left[E_b(T_i) - G_{k,T} \right] \tag{11}$$

$$G_{k,sol} = F_{k,sun} E_{sun}(\phi_s, \theta_s) + F_{k,a} E_{sol}(\phi_k, \theta_k) + \sum_{j}^{N_{kj}} F_{k,j} J_{j,sol} \tag{12}$$

$$G_{k,T} = F_{k,a} E_{bck}(\theta_k) + \sum_{j}^{N_{kj}} F_{k,j} J_{j,T} \tag{13}$$

Because of the inherent coupling of J_j and J_k:

$$J_{j,sol} = \rho_{j,S} \left[F_{j,sun} E_{sun} + F_{j,a} E_{sol}(\phi_j, \theta_j) + \sum_{k}^{N_{jk}} F_{j,k} J_{k,sol} \right] \tag{14}$$

$$J_{T,j} = \rho_{j,T} \left[E_b(T_i) + F_{j,a} E_{bck}(\theta_j) + \sum_{k}^{N_{jk}} F_{j,k} J_{k,T} \right] \tag{15}$$

these two equations are solved using a successive approximation iterative scheme. The solar-band equations are solved once at the start of each thermal solution (i.e., independent of temperature) and the thermal-band equations are solved after each iteration of the thermal conductance equation, producing a fully-coupled (implicit) thermal solution. Another advanced feature of ShipIR is the directional mapping of indirect solar irradiation. Figure 6 shows the prediction of an equivalent solar
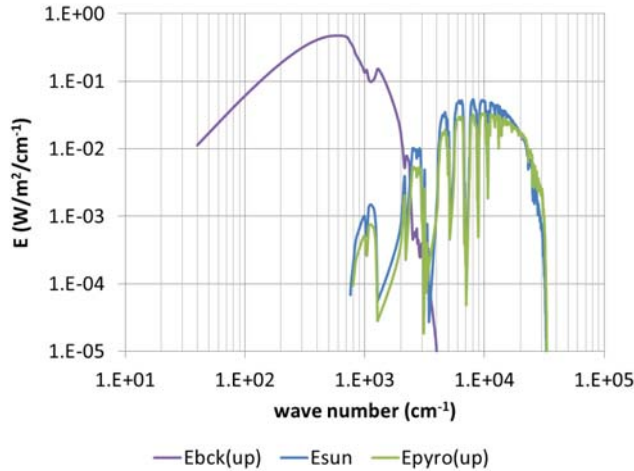
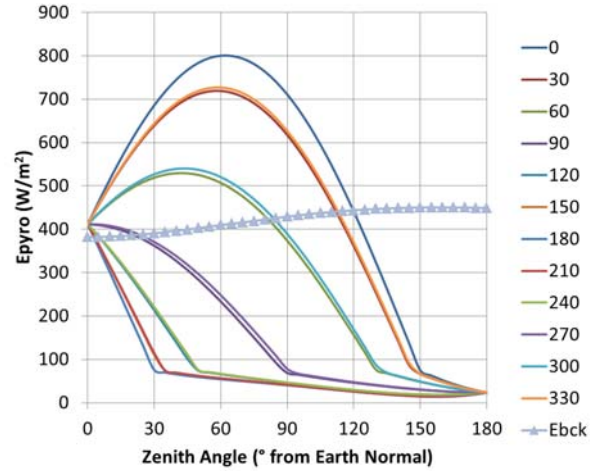**Figure 5**: Thermal and solar spectral irradiation from ShipIR.

Figure 6: ShipIR predicted pyrometer readings versus zenith at various azimuths (°CW from East).

pyrometer reading as a function of facet orientation (zenith, azimuth). The residual solar-scattering on the shaded side of an object (e.g., 50 W/m^2) is enough to produce a slightly positive contrast temperature between the surface and ambient air during daytime, instead of the slightly negative contrast temperature obtained at night or without this term modelled.

4.   SHIPIR/FLUENT INTERFACE

The functional interface between ShipIR and CFD for the Fluent software is shown in Figure 7. The process is initialized by a ShipIR model solution without CFD. This takes into account the thermal radiative background, the auto-generated ShipIR (external) convection model and any user-defined (internal) thermal boundary conditions. The output is a thermal system model (.tsm) file containing the wall boundary heat-flux data for input to CFD. The procedures used to interface the two codes are as follows: a single command-line shell program (cfd_rad) reads in the ShipIR model and a CFD surface mesh (.msh); maps each face in the CFD mesh to a ShipIR surface and associated plate node; and generates a set of heat flux data (*.dat) files containing the net heat flux from each wall face to the fluid. This is referred to as the flux mode of cfd_rad. A ShipIR analysis group is defined for each wall zone in the CFD surface mesh (with the same name). It contains the ShipIR surfaces associated with each wall zone. This not only simplifies the mapping search (by limiting the no. of facets to test in each zone), it also allows the user to clearly specify which side

Figure 7: Functional interface between ShipIR and Fluent.

of a two-sided (shadow) face is being used in each zone. Some modifications to the ShipIR model were required to segregate the heat-fluxes on each side of a conducting plate since the two sides share the same plate node. A separate optional input file (*_zones.dat) is used to specify the zone names in the mesh file. This file is used to handle Fluent exported meshes that do not contain any zone names.
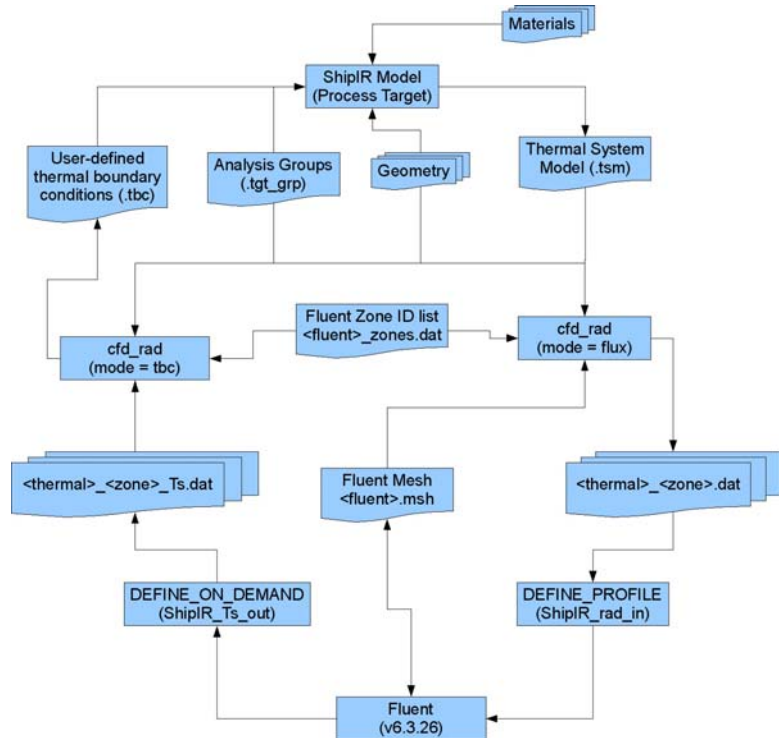
The next step involves setting up and processing the CFD model using the wall fluxes computed by ShipIR. For Fluent, a user defined function (UDF), ShipIR_rad_in, was created using the DEFINE_PROFILE framework of Fluent. The Fluent user must first compile the UDF library (source code provided), load the module into an active Fluent session, associate each thermal wall boundary with ShipIR_rad_in, and iterate the solver at least once with a non-zero UDF Profile Update Interval. Then, the CFD solution is iterated until convergence using the same heat-flux values, and a define_on_demand UDF (ShipIR_Ts_out) is used to export the wall and fluid temperatures to another set of data (*_Ts.dat) files, containing the integer ID, wall temperature and neighbouring fluid temperature for each wall face in the same zone.

The last step in the iteration process is to update the ShipIR convection boundary conditions based on the Fluent wall and fluid boundary temperatures. The shell program cfd_rad is used again, this time in tbc mode. Since the CFD mesh resolution is typically much higher than the ShipIR surface mesh, the wall and fluid temperatures are first area-averaged for each ShipIR node. The new convective heat transfer coefficient (h) and potentially a new fluid temperature node (T_f) are computed depending on whether the wall is heated or cooled (by the fluid), and whether the local Fluent fluid temperature is below or above the specified ShipIR fluid temperature (T_∞):

$$h_c = \begin{cases} \dfrac{\overline{q}_c}{\overline{T}_s - \overline{T}_f} & local \\[2ex] \dfrac{\overline{q}_c}{\overline{T}_s - T_\infty} & global \end{cases} \qquad (16)$$

A truth table (Table 3) describes the global versus local convection boundary condition logic. The end result is an auto-generated ShipIR thermal boundary condition (.tbc) file used to update the ShipIR thermal model and restart the iteration cycle with a new set of

Table 3: Differentiation between global and local convection.

Mode	Wall Conditions	Fluid Conditions	Convection
heating (q<0)	$T_p < \overline{T}_f$	$T_\infty < \overline{T}_f$	local
		$T_\infty \geq \overline{T}_f$	global
cooling (q>0)	$T_p > \overline{T}_f$	$T_\infty \leq \overline{T}_f$	global
		$T_\infty > \overline{T}_f$	local

heat-flux data files. The coupled solution typically converges in 5-6 iterations of this functional interface (ShipIR, cfd_rad, ShipIR_rad_in, Fluent, ShipIR_Ts_out, cfd_rad). Eventually, cfd_rad will be merged into the ShipIR framework (as an option) to avoid reloading and remapping the fluent mesh at each interval in the ShipIR and Fluent iteration. This data and mapping could be retained in active ShipIR memory until a different model geometry or CFD mesh is used.

5. RESULTS AND DISCUSSION

A scatter graph of Fluent vs ShipIR wall temperature after each iteration, shown in Figure 9, illustrates how the initial mismatch disappears with each iteration. The cumulative distribution function (CDF) of dT between the initial and final solutions, shown in Figure 10, highlights the tendency of ShipIR to predict both lower (dT<0) and higher (dT>0) convection values without the Fluent interface. These observations are further demonstrated in the long-wave infrared (LWIR) image output in Figures 11 and 12, and the long-wave and mid-wave polar signature plots in Figures 13 and 14. These clearly show that the uninsulated exhaust pipes are hotter in the initial ShipIR solution (dT<0), whereas the sun-heated area of the funnel is warmer in the coupled solution (dT>0). The mean and standard deviation between the initial and final polar signature plots, respectively, is 14% and 30% in the LWIR and 20% and 40% in the MWIR. These differences are significant and demonstrate the need to further validate the coupled solution.

In this simulation, the absolute wind speed and direction were chosen so that the relative wind would disperse the exhaust plume forward into the top area of the funnel mast. The absolute ship heading, date and time were chosen so that the sun would irradiate the area of the funnel in flow separation (i.e., leeward side of the funnel). These flow effects are best illustrated by plotting the air temperature contours from Fluent, as shown in Figures 15 through 17. With the two main propulsion diesels and gas turbine operating at full power, and their exhaust temperatures at 320°C and 440°C, respectively, the hot regions of the plume still keep clear of the ship structure. This is further demonstrated by the Fluent particle trajectories in Figure 18. The relative wind would have to be more directed towards the bow (0°) to maximize the potential
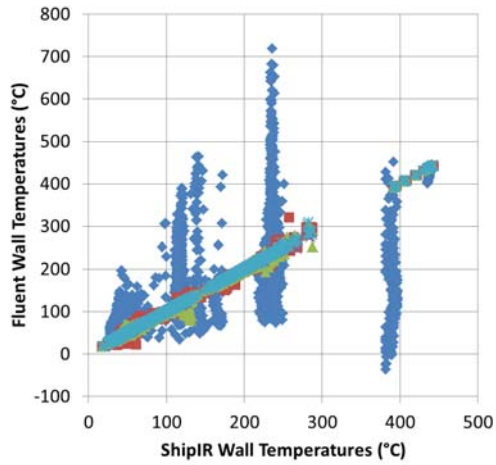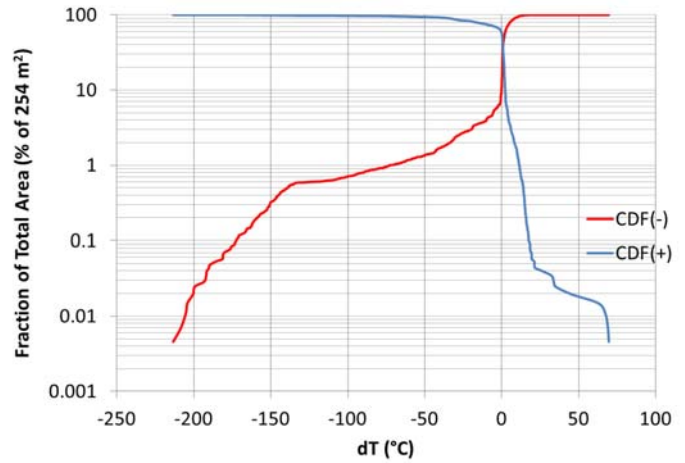
Figure 9: Fluent vs ShipIR wall temperatures.

Figure 10: Distribution of dT between initial and final solutions.

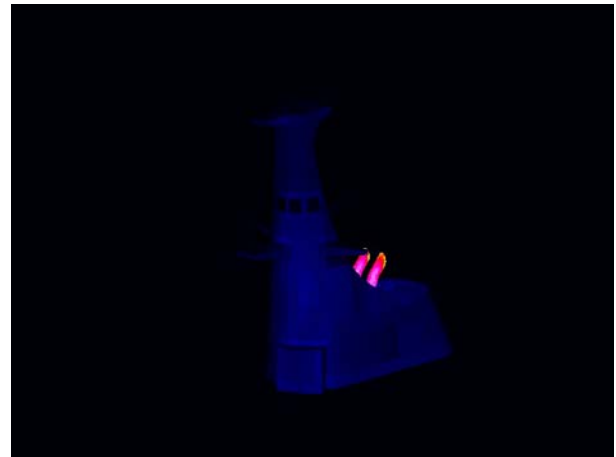**Figure 11**: LWIR image, ShipIR alone (36.3-232.5 W/m^2/sr).

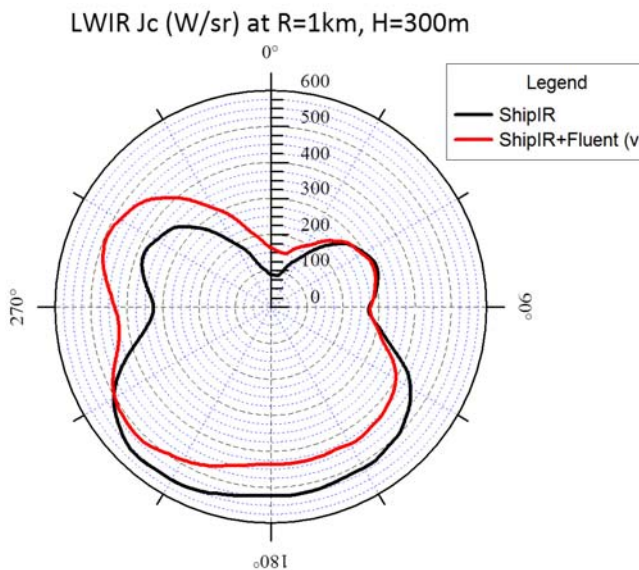**Figure 12**: LWIR image, ShipIR+Fluent (36.3-232.5 W/m^2/sr).
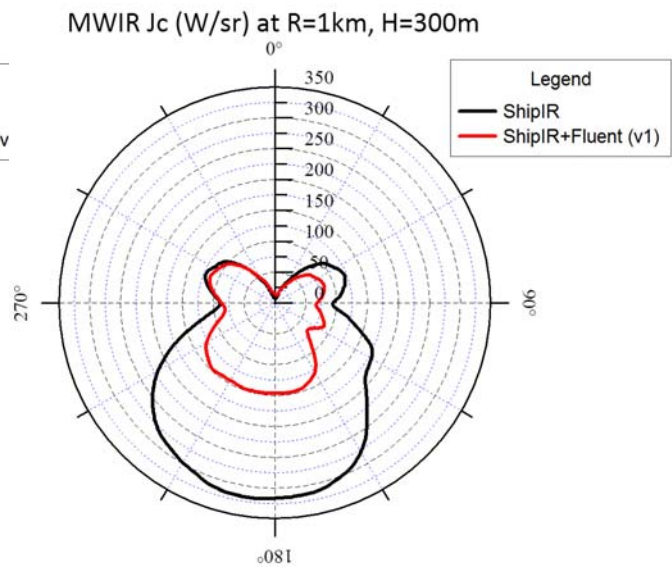

Figure 13: Polar plot of LWIR contrast intensity.

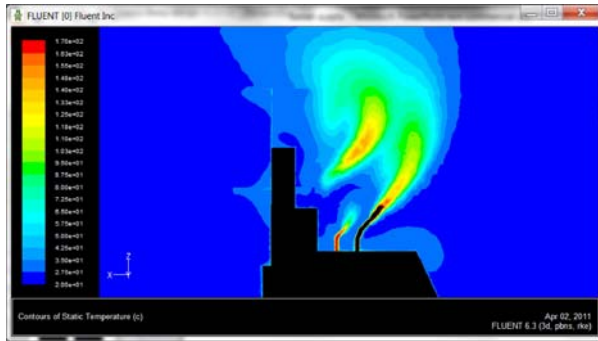**Figure 14**: Polar plot of MWIR contrast intensity.

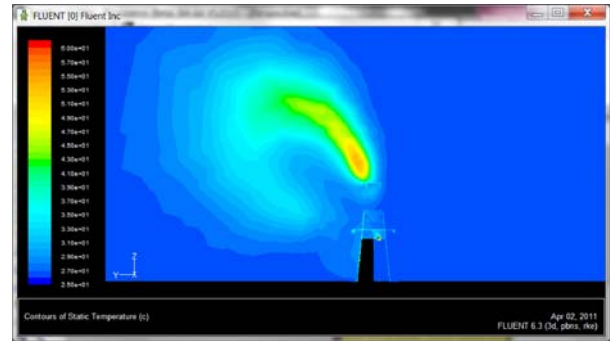**Figure 15**: Fluent temperatures in xz plane at y=0 m.

Figure 16: Fluent temperatures in yz plane at x=0.558 m.

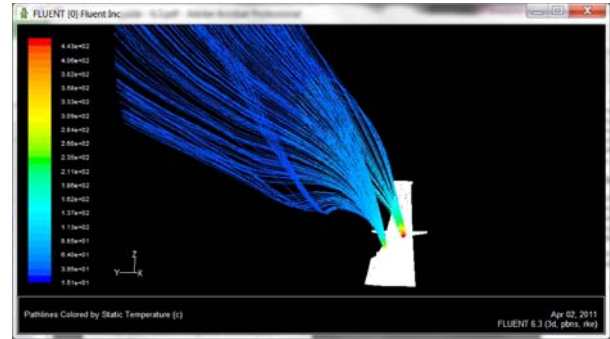**Figure 17**: Fluent temperatures in xy plane at z=13.0 m.

Figure 18: Fluent particle trajectories from the GT and MPDE.

for plume impingement. The area-weighted mean temperature difference (ΔT) between the local fluid temperature and the ambient air is only +2.1°C. Only 1.6 m^2 of the total 254 m^2 of surface area modelled required a local-area convection model, as outlined in Table 3.

6.   SUMMARY AND CONCLUSION

A new functional interface between ShipIR and CFD using Gridgen and Fluent has been presented. The Fluent surface and volume meshes were constructed from a ShipIR exported surface mesh using Gridgen (Pointwise). The results show a significant change in temperature and signature between the initial ShipIR and final ShipIR+Fluent solutions. The next steps are to construct a full-ship Fluent model of CFAV Quest, perform a sensitivity analysis on the Fluent modelling options, and conduct a full-ship measurement to validate the new solution.

7.   REFERENCES

1.   Cox, C. and Munk, W., "Measurement of the Roughness of the Sea Surface from Photographs of the Sun's Glitter," *J. Opt. Society Am*. 44, 838-850 (1954).
2.   Fraedrich, D., S., Stark, E., Heen, L.,T., and Miller, C., "ShipIR model validation using NATO SIMVEX experiment results," *Proc. SPIE* 5075, Targets and Backgrounds IX: Characterization and Representation, 49-59 (2003).
3.   Mermelstein, M., D., Shettle, E., P., Takken, E., H. and Priest, R., G., "Infrared radiance and solar glint at the ocean-sky horizon," *Appl. Opt*. 33 (25), 6022-6034 (1994).
4.   Ross, V. and Dion, D., "Sea surface slope statistics derived from sun glint radiance measurements and their apparent dependence on sensor elevation," J. Geophys. Res., 112, C09015, doi:10.1029/2007JC004137 (2007).
5.   Shaw, J.,A. and Churnsize, J.,H., "Scanning-laser glint measurements of sea-surface slope statistics," *Appl. Opt*. 36 (18), 4202-4213 (1997).
6.   Vaitekunas, D., A. and Fraedrich, D., S., "Validation of the NATO-standard ship signature model (SHIPIR)," *Proc. SPIE* 3699, Targets and Backgrounds: Characterization and Representation V, 103-113 (1999).
7.   Vaitekunas, D., A., "Validation of ShipIR (v3.2): methods and results," 1st International Workshop for IR Target and Background Modelling 27–30 June Ettlingen Germany (2005).